Research article

Economical magnetic activated carbon for methylene blue removal from water

Na Qin [a], Chengxuan Tian [a], Laura Carter [b], Dan Tao [a], Yuxin Zhou [a], Fan Zhang [a,b,*]

[a] College of Science, Nanjing Agricultural University, Nanjing 210095, China
[b] School of Geography, University of Leeds, Leeds LS2 9JT, UK

ARTICLE INFO

ABSTRACT

This study investigates an easy synthesis method of magnetic activated carbon (Fe_3O_4/AC) composites by ultrasonic mechanical blending of Fe_3O_4 particles and activated carbon (AC) powder at different mass ratios. The materials with the best performance were characterized by scanning electron microscope (SEM), energy dispersive spectroscopy (EDS), X-ray powder diffraction (XRD), specific surface and porosity analyzer (BET), hysteresis loop meter (VSM), thermogravimetric analysis (TGA), X-ray photoelectron spectroscopy (XPS). The as-prepared Fe_3O_4/AC was used to remove the contaminant methylene blue (MB) from solution. The effects of initial solution pH, material dosage, and temperature on MB removal were studied. A series of batch experiments demonstrated that the Fe_3O_4/AC with a mass ratio of Fe_3O_4 to AC = 1:5 showed a higher adsorption capacity of 251.3 ± 2.0 mg/g at 20 °C and pH = 6.5. Isotherm and kinetic studies indicated that the MB adsorption onto Fe_3O_4/AC was exothermic in a chemical monolayer adsorption process. The purification mechanism of Fe_3O_4/AC was investigated, FT-IR results showed that MB molecules adhered to Fe_3O_4/AC after purification. From the results of XPS full spectrum and high resolution spectrum, the possible purification mechanism is inferred as follows: electronic transfer between $=N^+$ in MB and C=O/C—O in Fe_3O_4/AC, as well as π-π interaction between the skeleton sheet of Fe_3O_4/AC and aromatic ring of MB. This study provides the theoretical reference and experimental basis for recovery and utilization of easily-obtained Fe_3O_4/AC to remove MB from wastewater.

1. Introduction

With the development of modern society, global water security is facing great challenges. More than 80 % of industrial wastewater containing pollutants is discharged into the environment without treatment [1]. The sources of Methylene Blue (MB) are primarily industrial processes where they are synthesized and then used as colorants or additives. Improper handling and disposal of MB-containing waste can lead to environmental contamination, especially in water. However, the occurrence of MB in environmental waters has gained increasingly attention as it is recalcitrant in nature and toxic which presents a risk to non-target organisms and the wider environment [2]. MB can cause eye burns, methemoglobinemia, cyanosis, convulsions, tachycardia, respiratory distress, skin irritation, and in more serious cases, gastrointestinal irritation, diarrhea, nausea, and vomiting in humans and animals [3], and it has been classified as one of the important pollutants. The dye-contaminated water can significantly affect aquatic life as well as human health even in small concentrations [4].

Wastewater treatment methods are generally divided into three categories: biological, chemical and physical methods. Physical methods mainly include adsorption, precipitation, filtration, membrane separation, ultrasonic gas vibration method, etc. Chemical methods mainly include advanced oxidation processes [5], electrochemical method. Adsorption is adsorption is a more mature, low-cost, easy to operate, widely applicable method, and the process is considered to be an efficient and inexpensive wastewater treatment method. Various removal strategies have been reported for MB in wastewater, including several physical removal methods, such as Perlite@GO, Bentonite SDBS-loaded composite, hydroxyapatite nanoparticles and corn husk waste [6–9]. Activated carbon (AC) had wide sources, low preparation cost and superior adsorption performance, which can be prepared from fruit shells, wood, waste straw, dead leaves, etc. Activated carbon has a rich pore structure. The mesoporous structure has been widely used for MB removal by providing a larger specific surface area, suitable pore size distribution and good pore connectivity [10–12], which positively affects adsorption. However, research has also shown that it is difficult to

separate AC from the solution after MB removal, and this has the potential to lead to secondary water pollution [13]. Magnetic composites are easy to separate from water after purifying dyes, so more magnetic adsorbents are used to treat dyes in printing and dyeing wastewater [14]. However, some magnetic materials are complicated to prepare, costly, or the adsorption capacity needs to be further improved, which limits their application. Therefore, exploring magnetic nanomaterials that are cheap, easy to obtain and easy to recycle has become a hot research topic. The combination of Fe_3O_4 nanoparticles and AC materials can effectively solve the problem and therefore, magnetic AC materials have gained increasing attention as a potential removal strategy for dye removal [15]. For example, a Xanthate functionalized magnetic activated carbon composite showed good removal capacity for several dyes, including MB [16]. Synthesized magnetic $MgAl_2O_4$-AC has also been shown to be an effective nano-photocatalyst for MB [17] as well as pineapple crown leaf heated at 500°C in reduced air conditions and converted to magnetic AC which has been shown to be efficient in the removal of methyl violet dyes[18]. Comparatively, the cobalt based metal organic framework supported on the magnetic ACs showed a maximum adsorption capacity of 112.3 mg/g for methylene blue [19]. These magnetic AC composites have the advantage of easy magnetic separation after dye removal. However, the laboratory preparation steps of the aforementioned adsorbents are highly demanding, and coupled with high material costs and environmental implications of the organic reagents as raw materials [20]. Therefore, it is important to develop an easier method to prepare magnetic activated carbon with low cost and energy requirements to meet the widespread need for effective dye removal [21].

Accordingly, an economic adsorbent for MB removal was synthesized and tested to understand its removal capacity of the cationic dye in solution. Short-term ultrasonic mechanical blending of commercial Fe_3O_4 nanoparticles (10–50 nm) and commercial AC with definite ratio in ethanol solution was used to prepare Fe_3O_4/AC composites. The materials with the best performance were characterized by scanning electron microscope (SEM), energy dispersive spectroscopy (EDS), X-ray powder diffraction (XRD), specific surface and porosity analyzer (BET), hysteresis loop meter (VSM), thermogravimetric analysis (TGA), X-ray photoelectron spectroscopy (XPS). The effects of dosage, adsorption time, initial concentration, temperature, and pH on the adsorption capacity of the Fe_3O_4/AC composites were systematically investigated. The adsorption kinetic and isotherm data in the removal process were modeled in detail and the interactions between the Fe_3O_4/AC and MB were further analyzed by FT-IR and XPS. To demonstrate the sustainability of this approach the stability and potential to recycle the Fe_3O_4/AC composites after MB removal was also assessed. In this study, a new type of magnetic activated carbon with excellent magnetic recovery was prepared in one step by a simple ultrasonic mechanical mixing the relative proportion of magnetic components and activated carbon. The economical magnetic activated carbon can be applied to purify methylene blue from wastewater.

2. Materials and methods

2.1. Materials and reagents

Commercial Fe_3O_4 nanoparticles with a diameter of 10–50 nm and commercial AC were purchased from Tianjin Seedior Company. Sodium hydroxide, methylene blue (MB), ethanol, hydrochloric acid were purchased from Shanghai Sinopharm Chemical Reagent Co, Ltd. (China). All the above reagents were analytical pure. Fig. S1 shows the chemical structure of MB.

2.2. Preparation of Fe_3O_4/AC composites

Five types of Fe_3O_4/AC composites with different mass ratios were prepared (1:3, 1:4, 1:5, 1:6, and 1:8; magnetic particles: activated carbon). Firstly, different doses of Fe_3O_4, 2.0 g AC powder, and 10 mL ethanol were added to 90 mL deionized water. Ultrasound stirring was used to blend this mixture for 30 min at room temperature and followed by magnetic separation which was used to obtain a black-colored solid product. Finally, the as-prepared magnetic Fe_3O_4/AC was thoroughly washed with deionized water and ethanol, and then dried at 50 °C for 3 h.

2.3. Instrument

The pH values of solutions were measured by a pH-meter (PHS-3 C, Jingke, Shanghai). The morphology of Fe_3O_4/AC was observed by SEM (Field Emission Scanning electron microscopy, Phenom Pro, Netherlands). The phase structures of the materials were studied by X-ray diffraction patterns (Miniflex600, Rigaku, Japan). The physical property measurement system was used to investigate the magnetic performance of Fe_3O_4/AC (Model-7404, Lake Shore, USA). The specific surface area of Fe_3O_4/AC was measured via Brunauer-Emmett-Teller (BET) while the microporous volume (Vmicro) was obtained via t-plot method. Thermal gravimetric analysis (TGA, NETZSCH STA 449F3) was performed in an inert dynamic atmosphere at a constant rate of 20 °C/ min from 30 °C to 1000 °C. The corresponding zeta potential (ZP) values of the materials were measured via a ZP analyzer (Malvern, Nano ZS, England). The dye concentrations were determined via an ultraviolet spectrophotometer (UV1800, Shimadzu, Japan). Fourier transform infrared (FTIR, Nicolet iS5, Thermo, USA) spectra with a scanning range from 400 to 4000 cm^{-1} at room temperature were recorded by using the KBr pellet method to study the functional groups of Fe_3O_4/AC before and after dye adsorption. X ray photo-electron spectroscopy (XPS) was conducted over a Thermo Scientific K-Alpha instrument. All XPS spectra have been calibrated by using the binding energy of C 1 *s* (284.8 eV) as the reference.

2.4. Adsorption experiments

MB was dissolved in deionized water to prepare a stock solution (initial MB concentration: 200 mg/L). To test the efficacy of MB removal from solution, 0.1 g Fe_3O_4/AC was added to 100 mL of dye solution (200 mg/L) in a beaker and stirred continuously with a machine. Experimental parameters including contact time (0–60 min), initial pH (5−11) of the dye solution, and temperature (5–45°C) were varied to test the effect of different experimental conditions on MB removal. Solution pH was adjusted using 0.1 M HCl or NaOH solutions to obtain the desired pH values. A required amount of Fe_3O_4/AC (0.02 g, 0.05 g, 0.1 g, 0.15 g, 0.2 g, or 0.5 g) was added to the synthetic MB solution (initial MB concentration: 200 mg/L reaction time: 60 min; solution volume: 100 mL; solution pH: 6.5; temperature: 25 °C) to evaluate the effect of adsorbent dosage. Different concentrations (50–500 mg/L) of MB solution were used to study the adsorption isotherm by 0.1 g Fe_3O_4/AC after 60 min at pH 6.5 and 25 °C. Adsorption tests were performed at 0.1 g Fe_3O_4/AC with three repetitions and the mean value of data was reported [22].

After each adsorption experiment, Fe_3O_4/AC was separated from the aqueous solution by a small neodymium magnet (diameter of 50 mm, thickness of 5 mm). A 4 mL aliquot of the residual solution was sampled by a pipette, and the residual concentration of MB in the sampled solution analyzed by a UV-Vis spectrophotometer at 664 nm. The adsorption amount was calculated using the difference in the dye concentration in the aqueous solution before and after adsorption:

$$q_e = \frac{(C_0 - C_e)V}{m} \tag{1}$$

where q_e is the equilibrium concentration of dye on the adsorbent (mg/ g); C_0 and C_e are the initial and equilibrium concentrations of dye solutions (mg/L), respectively; *V* is the volume of dye solution (L); and *m* is

the weight of the adsorbent (g) used.

2.5. Stability and reusability

The chemical stability of the Fe$_3$O$_4$/AC composite at different solution pH values of 5–11 was also investigated. Following one adsorption experiment, the Fe$_3$O$_4$/AC composite was also removed washed with ethanol and distilled water, dried at 60 °C for 6 h, and then weighed before being reused under the same exposure conditions to test reusability of the technique. All experiments were duplicated. Furthermore, the application of Fe$_3$O$_4$/AC for removing MB from natural water samples was tested.

3. Results and discussion

3.1. Characterization of Fe$_3$O$_4$/AC composites

Fig. 1 shows the SEM image and EDS results of the prepared Fe$_3$O$_4$/AC. In Fig. 1a, the surface of AC is rough and porous, which is favorable for adsorption. And there are also many clusters of polymers on the surface of AC [23], indicating that Fe$_3$O$_4$ may be successfully loaded onto the surface of activated carbon. It can be seen that those clusters consisted of irregular Fe$_3$O$_4$ nanoparticles with an average particle size of 100–800 nm. Fig. 1b is the SEM image of Fe$_3$O$_4$/AC after adsorption, there is no obvious change compared with that before adsorption. This is consistent with the particle size distribution result of the range of
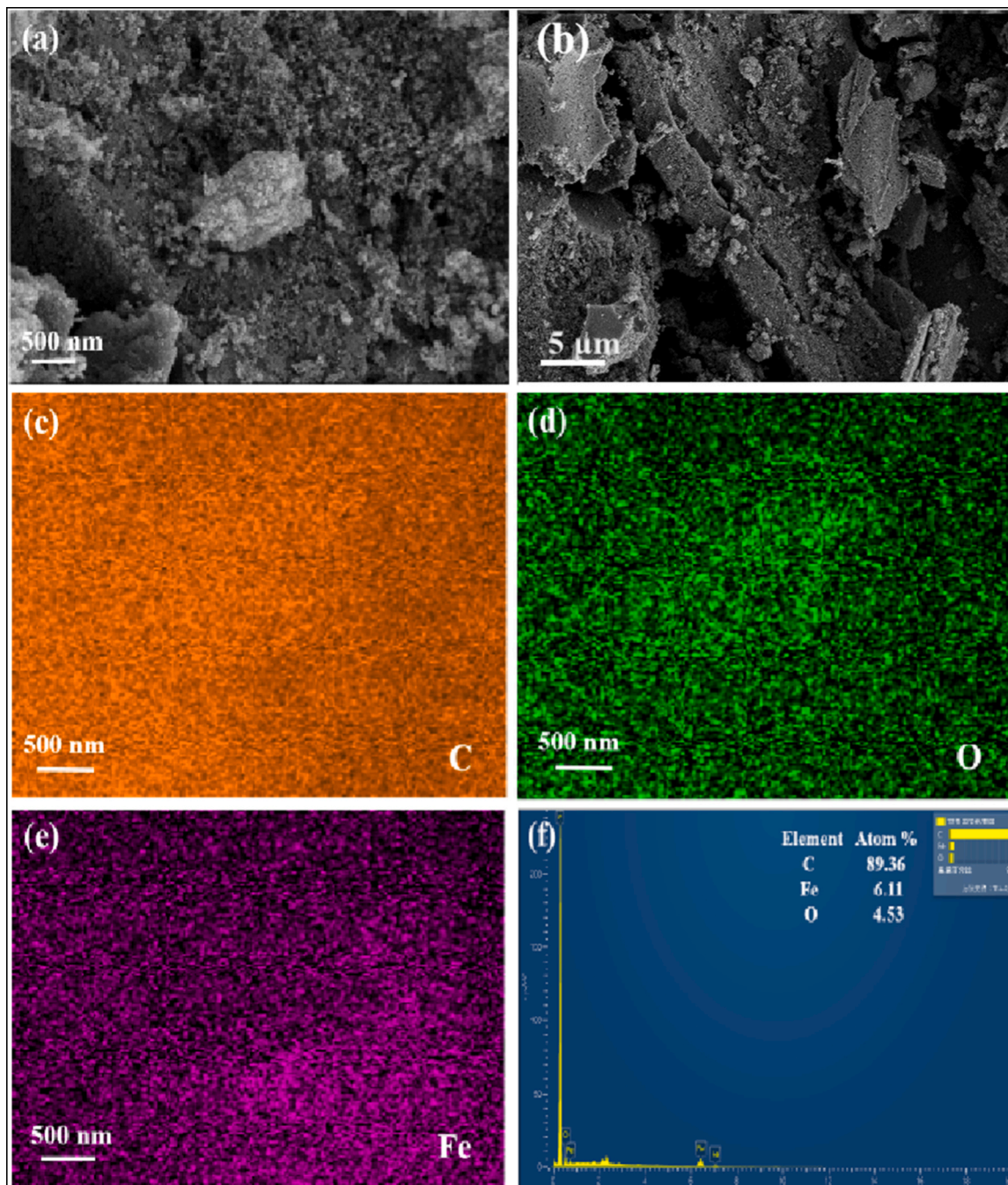
Fig. 1. (a) SEM image of Fe$_3$O$_4$/AC; (b) SEM image of Fe$_3$O$_4$/AC after the adsorption process; corresponding element mapping of (c) C (d) O, and (e) Fe in Fe$_3$O$_4$/AC, (f) EDS results.

200–600 nm (Fig. S2). As shown in the element mapping, C, O and Fe were observed and evenly distributed in the mesoporous structure of Fe_3O_4/AC. The presence of Fe in Fig. 1f (with an atomic content of 6.11 %) ensured the magnetic property of the Fe_3O_4/AC composites. Fig. 2a shows the XRD results of Fe_3O_4/AC compared with pure Fe_3O_4 and AC. The $2\theta = 44.5°$ peak in Fe_3O_4/AC can be ascribed to corresponded to (221) of AC. The characteristic peaks at $2\theta = 35.5°$, 37.1°, 57.3°, and 62.9° in Fe_3O_4/AC match with diffraction planes of (220), (311), (511), and (440) in XRD patterns of Fe_3O_4[24], respectively. As shown in Fig. 2b, the maximum value of saturation magnetization of Fe_3O_4/AC was 20.67 emu/g, which lead to the rapid magnetic separation (30 seconds) by a magnet, as indicated in the inset picture. In addition, Fe_3O_4/AC did not show any coercivity (Hc) or magnetization remanence (Mr), suggesting that the material is superparamagnetic and that it can be effectively separated from solution by an external magnetic field [25]. The N_2 adsorption-desorption isotherms and pore size distribution (PSD) curves of Fe_3O_4/AC are shown in Fig. 2c. It can be obtained that the Fe_3O_4/AC composites appear as typical type IV adsorption isotherms [26]. The specific surface area measured using BET analysis was 420.36 m^2/g with mesoporous structure, and the total pore volume was 0.496 cm^3/g. The average pore diameter was calculated to be 4.77 nm according to the pore distribution. According to the latest IUPAC classification, the hysteresis loop in this absorption-desorption isotherm corresponds to type H3. There is no obvious saturation adsorption platform in the H3 hysteresis isotherm, which indicates that the mesoporous structure is very irregular [27]. The TGA analysis of Fe_3O_4/AC was investigated and presented in Fig. 2d. The thermal gram of Fe_3O_4/AC gave three regions of weight loss. The first weight loss was may be due to the evaporation of water or alcohol from Fe_3O_4/AC. The second weight loss can be attributed to the breakdown of organic compounds in the AC and their conversion into gas. Finally, the degradation of unstable structure of Fe_3O_4/AC may result in the third weight loss [28]. The chemical stability of Fe_3O_4/AC in different pH solutions was also investigated (shown in Fig. S3). The weight loss of Fe_3O_4/AC in the pH range of 5–11 was less than 10 %, indicating that they can be stable in most solutions and demonstrating their potential to remove contaminant dyes across a wide pH range of environmental media.

3.2. Removal properties of materials for MB solution

3.2.1. Dye adsorption abilities of Fe_3O_4/AC with different magnetic content

The addition of Fe_3O_4 to AC plays an important role in magnetic separation of AC from solution after dye removal to avoid potential secondary pollution in the water system. In addition, Fe_3O_4/AC exhibited better hydrophilicity performance than pure AC composites (inner picture in Fig. 3a), which may enhance the contact of AC with dyes in solution. However, there is the potential that the Fe_3O_4 nanoparticles may block some of the mesopores in AC, which would lead to a decreased removal ability. Therefore, different magnetic content of Fe_3O_4 was incorporated into AC to better understand the influence of the Fe_3O_4 nanoparticles on MB removal (Fig. 3b). Notably, the Fe_3O_4/AC composites with Fe_3O_4 to AC (mass ratio) = 1:5 showed a high adsorption capacity of 136 mg/g within 60 min. Therefore, subsequent experiments focused on Fe_3O_4/AC with the mass ratio of 1:5.

The impact of changing pH on adsorption capacity was examined and is presented in Fig. 4a. With the increase of pH from 5 to 7, the removal percent of MB dye increased slightly with the highest capacity of MB removal (150 mg/g) obtained at pH 6–7, indicating the suitability in treating natural waters. MB can be present in aqueous solutions as cationic species (MB^+) and as undissociated molecules (MB^0), however
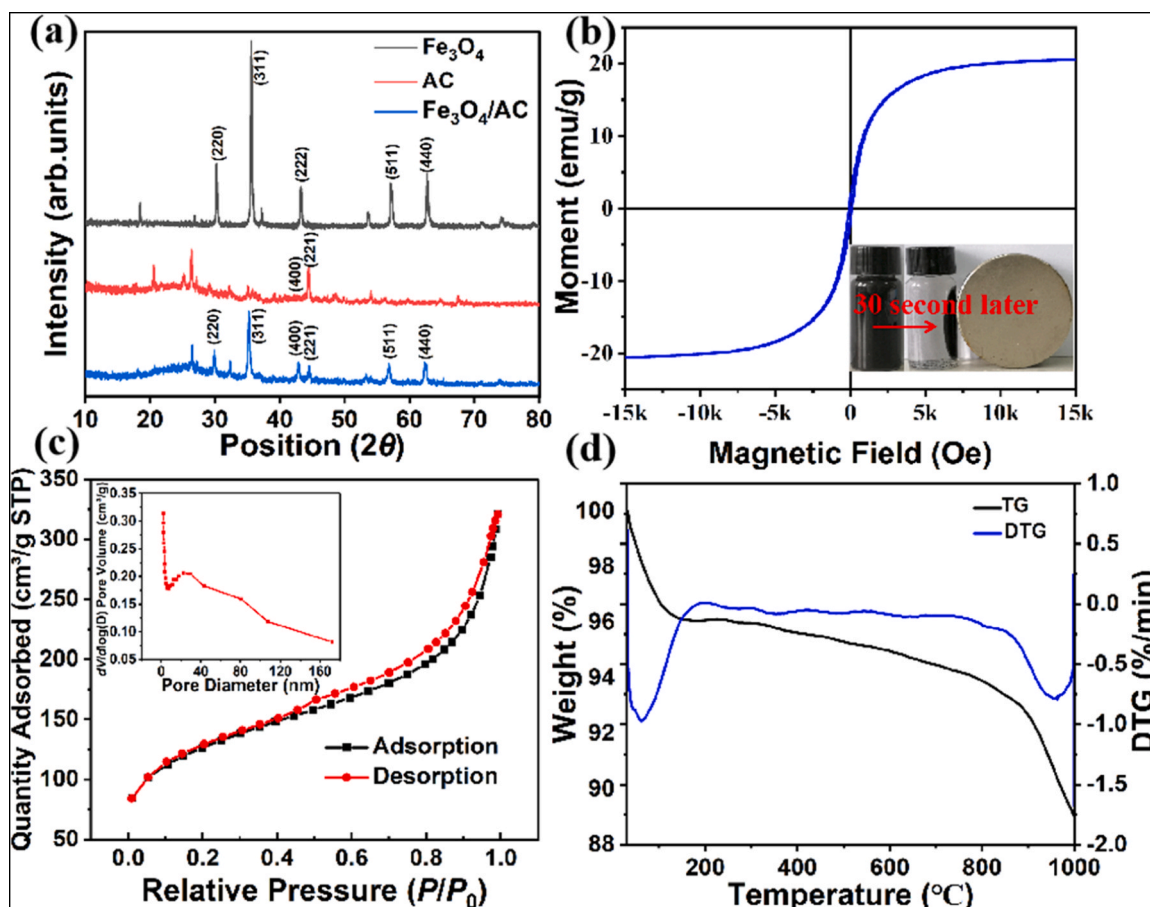
Fig. 2. (a) XRD patterns of Fe_3O_4, AC and Fe_3O_4/AC; (b) magnetic result; (c) BET result and (d) TGA curves of Fe_3O_4/AC.
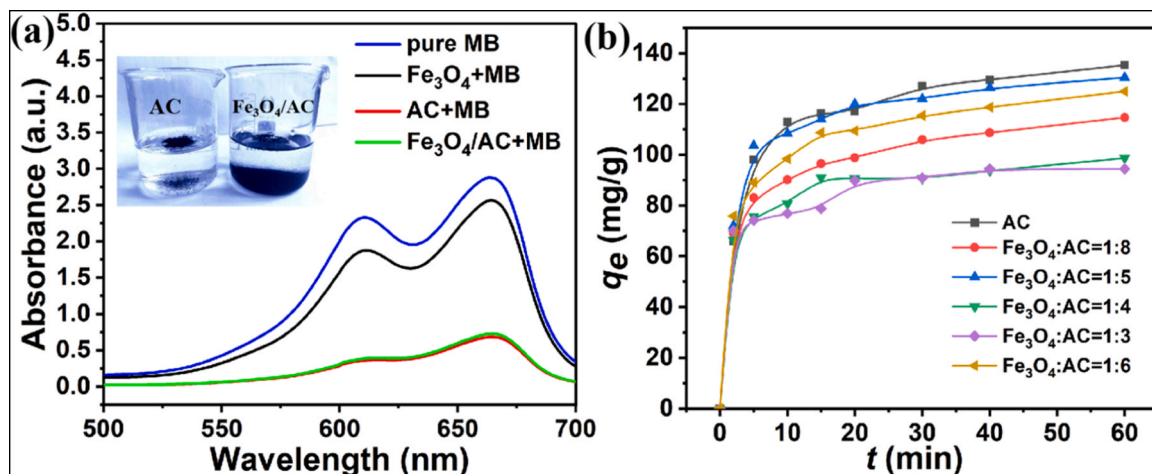
Fig. 3. (a) The adsorption capacity of Fe_3O_4, AC and Fe_3O_4/AC for MB solution ($C_0 = 200$ mg/L, dosage = 1.0 g/L, 25 °C, 60 min, and pH = 6.5) (inset: water solubility of AC and Fe_3O_4/AC). (b) The adsorption capacity of Fe_3O_4 with AC at different ratios for MB ($C_0 = 200$ mg/L, dosage = 1.0 g/L, 25 °C, and pH = 6.5).
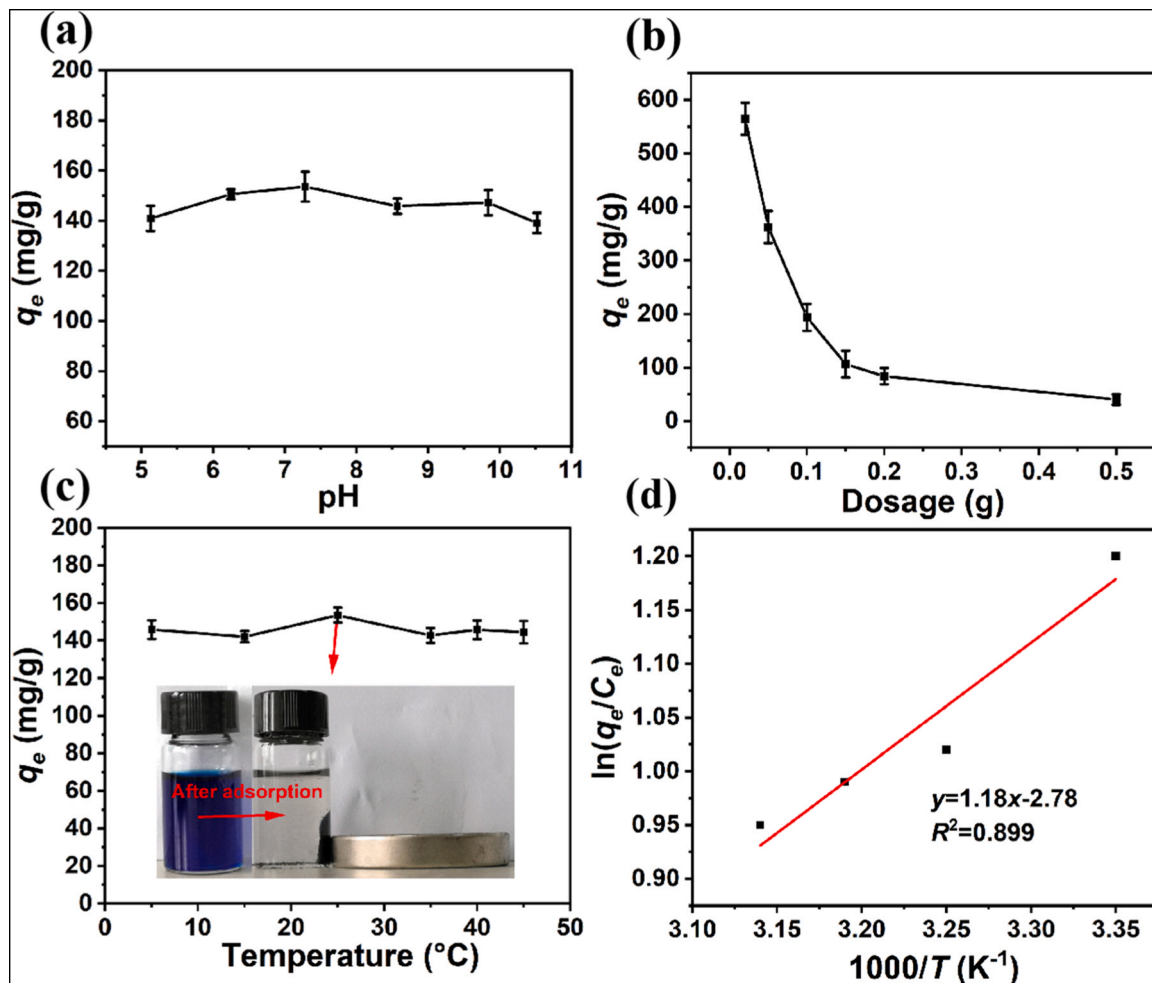
Fig. 4. Removal effects of MB solution by Fe_3O_4/AC at different (a) initial pH ($C_0 = 200$ mg/L, 60 min, dosage = 0.1 g/L, 25℃); (b) adsorbent dosage ($C_0 = 200$ mg/L, 60 min, pH = 6.5, 25℃); (c) temperature values ($C_0 = 200$ mg/L, 60 min, dosage = 0.1 g/L, pH = 6.5); (d) Van't Hoff plots for the adsorption of MB onto Fe_3O_4/AC.

MB^+ is practically the only species present in solution at pH > 6 [29]. The zeta potential of the Fe_3O_4/AC composite at various pH values is illustrated in Fig. S4. The pH at point of zero charge (pH_{PZC}) is 6.5. It demonstrates that at pH > pH_{PZC} (6.5), the negative charge on the

surface of the Fe_3O_4/AC may be suitable to adsorb cationic dyes. However, at pH < 6, excess H ions compete with cations on the dye for adsorption sites [30]; at pH > 7, the hydroxide of solution can compete with negatively charged Fe_3O_4/AC, to attract cationic dye molecules,

leading to the decreased adsorption capacity of Fe₃O₄/AC. Therefore, a pH of 6.5 was fixed to investigate the adsorption of MB in the following experiments.

Different Fe₃O₄/AC dosages (0.020 g, 0.050 g, 0.100 g, 0.150 g, 0.200 g and 0.500 g) were added into MB solution and examined to understand how concentration of the magnetic adsorbent can influence MB removal capacity (showed in Fig. 4b). The appearance of exponentially decreasing curve implied the decreased amount of dye (per unit weight of adsorbent) with the increase of adsorbent dosage, resulting in a prominent decrease in adsorption capacity [31]. This can be explained by the fact that when the surface of Fe₃O₄/AC is saturated with dye molecules, by increasing the adsorbent dose in the solution, adsorptive sites that require higher energy to adsorb pollutants would not be in contact with dye molecules, resulting in reduced adsorption capacity. Thus, a dosage of 0.1 g/L adsorbent was selected to be the standard dosage in the following experiments.

The uptake capacity of Fe₃O₄/AC for MB in the result of temperature ranging from 5 ℃ to 45 ℃ was shown in Fig. 4c. At the low temperature less than 15℃, both Fe₃O₄/AC and MB need more energy to start the molecular motion, leading to the slightly lower adsorption capacity. The high capacity of 153.560 mg/g was obtained at 25 °C. Clean water after adsorption and easy magnetic separation of Fe₃O₄/AC were observed (inner picture in Fig. 4c). After 25 °C, the adsorption capacity decreases slightly with the increase of temperature, indicating that the adsorption process may be an exothermic process. This is beneficial and supports the practical application of this technology in natural environments such as rivers, as no further energy is needed to initiate the adsorption process. Therefore, the following studies for MB adsorption were carried out at room temperature (approximately 25 °C) without energy application.

To further determine the effect of temperature on MB adsorption by Fe₃O₄/AC, the values of ln (q_e/C_e) at 25 °C, 35 °C, 40 °C, and 45 °C were treated according to Van' t Hoff equation [32]

$$ln \frac{q_e}{C_e} = -\frac{\Delta H}{RT} + \frac{\Delta S}{R} \tag{2}$$

where R is the universal gas constant (8.314 J/mol/K) and T is the absolute temperature (in Kelvin). Plotting ln(q_e/C_e) against $1/T$ gives a straight line ($y = 1.18x - 2.78$) with slope and intercept equal to -$\Delta H/R$ and $\Delta S/R$, respectively, as described in Fig. 4d. The negative value of ΔH (shown in Table S1, -9.81 ± 0.56) shows the exothermic nature of this adsorption process, implying that the adsorption is more favorable at comparatively low temperatures [33].

In addition, the negative entropy value (ΔS, -23.11 ± 1.34 J/mol/K) indicates that the randomness of the solid-solute interface is reduced by

the formation of an activated complex, which reflects the affinity of the Fe₃O₄/AC for MB dye [34]. Gibbs free energy of adsorption (ΔG) was calculated from the following equation:

$$\Delta G = \Delta H - T\Delta S \tag{3}$$

The negative values of ΔG (-2.46 ~ -2.92 kJ/mol) in Table S1 show the spontaneous nature of the binding process at 25 °C, 35 °C, 40 °C, and 45 °C [35].

3.2.2. Adsorption kinetics

To investigate the adsorption kinetics of the prepared Fe₃O₄/AC composite, pseudo-first-order (Fig. S5), pseudo-second-order (Fig. S6), intra-particle diffusion (Fig. S7) and liquid film diffusion (Fig. S8) kinetic models were used to evaluate the adsorption kinetic data of Fe₃O₄/AC toward MB (Fig. 5). The adsorption rate is assumed according to these different models [36]. A chemical adsorption mechanism including electron sharing or electron transfer between adsorbent and adsorbate controls the process of adsorption for pseudo-second-order kinetic model [37]. Intra particle diffusion mechanism can be identified by the intra particle diffusion model, which can explore how diffusion resistance affects the adsorption process. The last kinetic model is liquid film diffusion model, which assumes that the adsorbate molecule flows through a liquid film surrounding the adsorbent. This step is considered to be the rate-controlling step in the adsorption process [38]. The equations of the four models are as follows.

The pseudo-first-order kinetic equation [39]:

$$\ln(q_e - q_t) = \ln q_e - k_1t \tag{4}$$

The pseudo-second-order kinetic model [40]:

$$\frac{t}{q_t} = \frac{1}{k_2q_e^2} + \frac{t}{q_e} \tag{5}$$

The intra-particle diffusion model [41]:

$$q_t = k_{id}t^{0.5} + C \tag{6}$$

The liquid film diffusion model [42]:

$$-\ln(1-F) = k_Ft + C \tag{7}$$

$$F = \frac{q_t}{q_e} \tag{8}$$

where q_e (mg/g) is the adsorption capacity at equilibrium. q_t (mg/g) is the adsorption amount at time t (min). k_1 (g/mg min) is the rate constant of pseudo-first-order. k_2 (g/mg min) is the rate constant of pseudo-
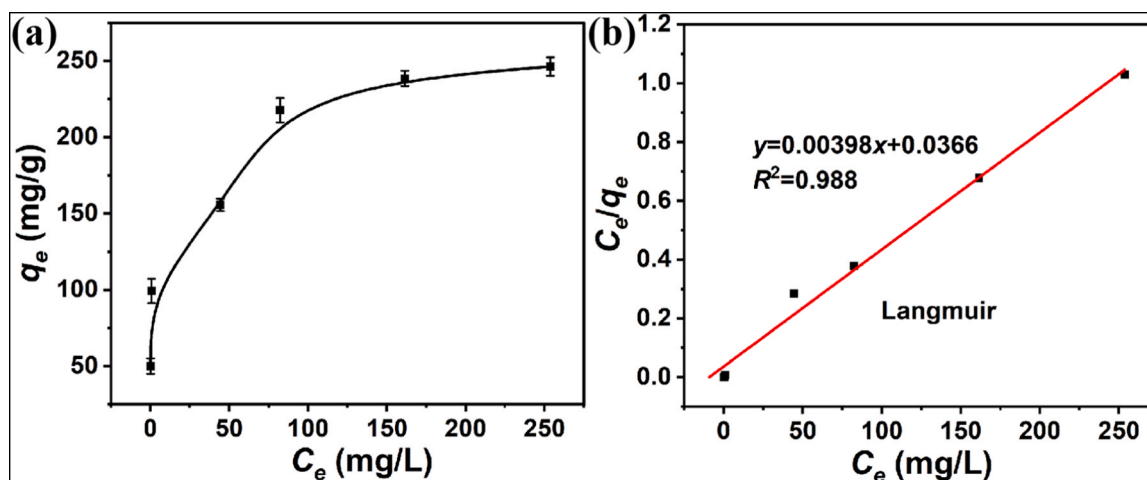
Fig. 5. (a) Adsorption dependency between C_e and q_e of MB onto Fe₃O₄/AC (dosage = 1.0 g/L, 60 min, 25 ℃, and pH = 6.5); (b) Linear fitting curves of Langmuir model of Fe₃O₄/AC (dosage = 1.0 g/L, 60 min, 25 °C, and pH = 6.5).

second-order. k_{id} (mg/g min$^{0.5}$) and k_F (min^{-1}) are the rate constant of intra-particle diffusion and liquid film diffusion, respectively. C (mg/g) is intercept of intra-particle diffusion and liquid film diffusion. The values of correlation coefficients (R^2) and other relative parameters were calculated from each model presented in Table 1 and Table S2. The value of R^2 is used to check the reliability of each model. The value of R^2 calculated from pseudo-second-order (PSO) model is higher than that of pseudo-first-older model. The adopting of the kinetic behavior of the adsorption process from the PSO model shows that the adsorption of MB is chemical, electrostatic, and chelate surface adsorption, and the reactions on the surface may be limit the speed of the process and govern the adsorption mechanism of MB[43]. Moreover, the calculated value of equilibrium adsorption capacity obtained from the pseudo-second-order kinetic equation is 251.300 mg/g, and implied that the adsorption capacity of Fe$_3$O$_4$/AC to MB was viable.

Fig. S7 shows the plot of intra-particle diffusion model for MB presenting a multi-linear relationship of which the adsorption process can be divided into three stages [41,42]. The first step is the immediate diffusion process. In this step, a large amount of MB dye was adsorbed from aqueous solution to Fe$_3$O$_4$/AC surface immediately since there were a large number of free adsorption sites on the materials. As a result, the rate constant ($k_{id.1}$) of this step was the highest. The second step was the intra-particle diffusion. In this step, MB molecules diffused into the internal pores of Fe$_3$O$_4$/AC when the adsorption sites of exterior surface reached saturation, leading to a moderate decreased diffusion rate of $k_{id.2}$ due to the increased resistance. The last step was equilibrium stage. In this step, there were few adsorption sites left on the materials and low residual concentration of MB in solution, leading to the rate constant ($k_{id.3}$) close to zero. Therefore, the first step and the second step were the rate-determining and rate-influencing steps in the adsorption process of MB by Fe$_3$O$_4$/AC. Notably, all the values of C referring to the boundary layer thickness were not equal to zero as shown in Table 1, implying that intra-particle diffusion was not the only rate-control mechanism in the process of adsorption [42,44]. As shown in Fig. S7 and Fig. S8, the calculated values of R^2 from the intra-particle model and liquid film diffusion model were both appropriate, suggesting that these two types of diffusion processes controlled the rate of dye adsorption onto our synthesized materials individually and collectively. Moreover, these two diffusion models ensure the adsorption procedure properly fits with pseudo-second-order kinetics [45].

The activation energy of MB adsorption onto Fe$_3$O$_4$/AC was calculated using the rate constant of pseudo-second order kinetic (k_2) values at 288, 298, 308 and 318 K as specified by the Arrhenius relation equation in the following:

$$\ln k_2 = \frac{E_a}{R}\left(\frac{1}{T}\right) + constant \tag{9}$$

Where E_a is the activation energy in kJ/mol. The E_a value was estimated from the slope of the Arrhenius plot of $\ln k_2$ versus $1/T$. The E_a values between 5 and 40 kJ/mol assume physisorption whereas larger E_a values between 40 and 800 kJ/mol indicates chemisorption [42]. As shown in Table 2, the calculated value of E_a from the slope depicted in Fig. S9 was 20.550 kJ/mol. The activation energy data assumes that the removal process is primarily physisorption (non-specific adsorption) rather than chemisorption [46]. This may be beneficial for Fe$_3$O$_4$/AC to be easily reclaimed and reused.

Table 2
Pseudo-second-order kinetic parameters at 288, 298, 308 and 318 K for removing MB by Fe$_3$O$_4$/AC.

Temperature (K)	pseudo-second-order			E_a (kJ/mol)
	k_2(g/(mg·min))	q_e (mg/g)	R^2	
288	0.007	141.000	0.999	20.550
298	0.006	251.300	0.999	
308	0.004	150.800	0.999	
318	0.003	148.100	0.999	

3.2.3. Adsorption isotherm

The interactive behavior between adsorbate and adsorbent can be described by adsorption isotherm. The relationship between C_e and q_e of MB adsorbed onto Fe$_3$O$_4$/AC was presented in Fig. 5a. The isotherm is I-type, revealing that the synthetic Fe$_3$O$_4$/AC composites have high affinity to MB molecules. In the range of low concentration, the values of q_e for MB increased linearly when the initial concentrations increased. However, when the concentration increased to a certain value, there were not sufficient vacant adsorption sites on Fe$_3$O$_4$/AC for excess MB molecules, which lead to the retarding of the linear growth [44]. Langmuir model, Freundlich model and Temkin model were used to further investigate the adsorption as expressed by the following Eqs. 10–12.

Langmuir isotherm model [28]

$$\frac{C_e}{q_e} = \frac{1}{K_L q_m} + \frac{C_e}{q_m} \tag{10}$$

Freundlich isotherm model [47]

$$\log q_e = \frac{1}{n}\log C_e + \log K_F \tag{11}$$

Temkin isotherm model [48]

$$q_e = B_1 \ln K_T + B_1 \ln C_e \tag{12}$$

where C_e (mg/L) is the equilibrium concentration of dye solution. q_m (mg/g) is the maximum adsorption capacity. K_L (L/mg) is the equilibrium adsorption constant for Langmuir isotherm model. K_F (L/mg) is related to the magnitude of adsorption driving force for Freundlich isotherm model. $1/n$ implies the degree of nonlinearity between solution concentration and adsorption [48]. K_T (L/mg) is the equilibrium binding constant corresponding to the maximum binding energy for Temkin isotherm model. Constant B_1 is related to the heat of adsorption.

The experimental data and non-linear fitting curves of these models were depicted in Fig. 5b, Fig. S9 and Fig. S10, and the corresponding parameters were listed in Table 3. Results show, the Langmuir model was more suitable than other models to fit the experimental data due to the high R^2 value. Therefore, the adsorption of MB may occur at specific adsorption sites forming monolayer adsorption on the homogeneous surface [49]. In addition, adsorbed MB molecules have no interaction between each other and the binding sites on the materials have the same affinity for MB. The maximum adsorption capacity of Fe$_3$O$_4$/AC in this work was calculated from the Langmuir model and shown in Table 3. Interestingly, the calculated capacity of 251.300 mg/g for Fe$_3$O$_4$/AC is higher than some previous reports for MB removal (Table 4).

The results of isothermal, kinetic and thermodynamic studies indicate that chemical interactions and physical bonding are established during the adsorption of MB by Fe$_3$O$_4$. In other words, chemisorption

Table 1
Kinetic parameters for removing MB by Fe$_3$O$_4$/AC.

Adsorbent	intra-particle diffusion						liquid film diffusion					
	k_{id} (mg/g min$^{0.5}$) C (mg/g)						R^2			k_F (min^{-1})	C	R^2
	$k_{id.1}$	$k_{id.2}$	$k_{id.3}$	C_1	C_2	C_3	R_1^2	R_2^2	R_3^2	0.041	1.580	0.940
Fe$_3$O$_4$/AC	7.220	4.730	1.470	111.500	122.060	143.280	0.980	0.843	0.843			

Table 3

Isotherm parameters for removing MB by Fe$_3$O$_4$/AC.

Adsorbent	Langmuir				Freundlich			Temkin		
	q_m (mg/g)	K_L (L/mg)	R_L	R^2	K_F(mg/g)/(mg/L)$^{1/n}$	$1/n$	R^2	K_T (L/g)	B_1	R^2
Fe$_3$O$_4$/AC	251.300	0.110	0.035	0.988	91.620	0.181	0.964	117.230	22.810	0.930

Table 4

Comparison of Fe$_3$O$_4$/AC with other adsorbents for MB.

Materials Materials	q_e (mg/g)	References
Magnetic rectorite/iron oxide	31.180	[50]
Neem leaves activated carbon	132.520	[51]
MWCNTs/Gly/β-CD	90.900	[52]
PET carbon	33.400	[53]
Ni$_{0.5}$Zn$_{0.5}$Fe$_2$O$_4$	47.700	[54]
Fe$_3$O$_4$@GPTMS@Lys	134.000	[55]
Fe$_3$O$_4$/AC	251.300	This paper

and physisorption act simultaneously through various mechanisms such as electrostatic interactions, ion exchange, pore saturation and surface complexation in the adsorptive removal of MB [56].

3.3. Mechanism of removal

Fig. 6 present the FT-IR spectrum of pure MB, dye-free and dye-adsorbed of synthetic Fe$_3$O$_4$/AC. For MB, the spectrum showed peaks at 892 cm^{-1}, 1498 cm^{-1}, 1627 cm^{-1} and 2270 cm^{-1} corresponding to the C—H (out-of-plane bend in aromatic rings) [57], the aromatic rings (C=C), C=N [58] and the C—H distortion tensile vibration of MB [59], respectively. For Fe$_3$O$_4$/AC, the spectra showed the peak at 767 cm^{-1}, 1363 cm^{-1} and 1598 cm^{-1} corresponding to the Fe—O stretching vibration peak, existence of asymmetric stretching vibration of C—O groups [60] and C=C or C=O groups [61] of Fe$_3$O$_4$/AC [62], respectively. These characteristic peaks of Fe$_3$O$_4$/AC have no obvious changes before and after adsorption. However, there is a new peak at 1627 cm^{-1} for C=N that appears in Fe$_3$O$_4$/AC after adsorption, indicating the existence of MB in the used Fe$_3$O$_4$/AC.

To further study the mechanism of the adsorption process, the XPS spectra of survey and high-definition scans of the key elements on the surface of pristine and used Fe$_3$O$_4$/AC were obtained and shown in Fig. S11 and Fig. 7. It can be seen from Fig. S11 that the C, O, N and Fe
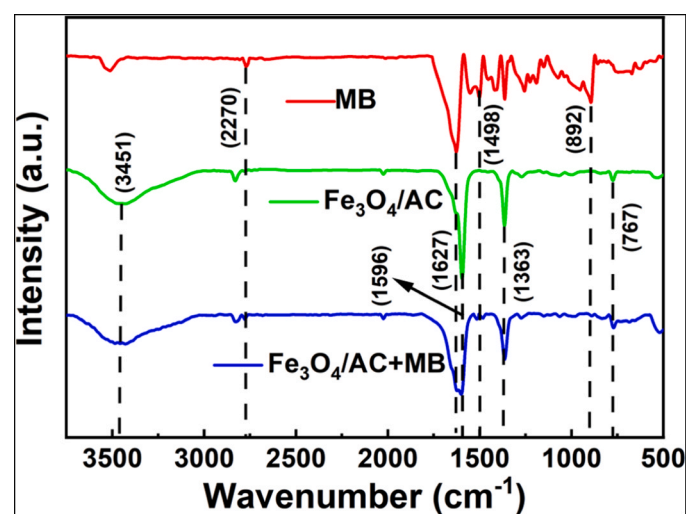
Fig. 6. FT-IR spectra of MB, the Fe$_3$O$_4$/AC (Fe$_3$O$_4$: AC = 1:5) samples before and after the absorption (C_0 = 200 mg/L, 25 °C, pH = 6.5, adsorbent = 1.0 g/L, 60 min).

were detected in pristine and used Fe$_3$O$_4$/AC. Especially, the N 1 s peak of Fe$_3$O$_4$/AC with MB loaded becomes relatively stronger than that of pristine Fe$_3$O$_4$/AC, which can be due to the appearance of adsorbed MB on the surface of reclaimed Fe$_3$O$_4$/AC. This result is consistent with FT-IR results.

The deconvolution of C 1 s spectra in MB-loaded Fe$_3$O$_4$/AC produces three peaks as shown in Fig. 7b. The first peak is at 284.72 eV corresponding to C—C/C=C species. The second peak is at 285.83 eV corresponding to C—O species. The third peak is at 289.85 eV corresponding to C=O species [63]. In this spectrum, an obvious shift from 289.85 eV to 289.40 eV is also observed in the peak of C=O. And the peak of C—O also shows an insignificant shift from 285.83 eV to 285.61 eV, suggesting the electronic transfer occurred in C=O/C—O of Fe$_3$O$_4$/AC. No obvious shift of C—C/C=C is observed. At the same time, the percentage of C—C/C=C peak in total peak of C 1 s descended from 57.92 % to 44.56 % after adsorption which may be contributed to the π-π interaction between the aromatic rings of MB and skeleton sheet (C—C/C=C) of Fe$_3$O$_4$/AC [64].

The high-resolution spectrums for Fe 2p of Fe$_3$O$_4$/AC before and after adsorption to MB are shown in Fig. S12 and Fig. S13, respectively. The core level spectra of Fe$_3$O$_4$ exhibit two broad peaks at about 711.00 eV and 724.60 eV, which can be assigned for the Fe 2p$_{3/2}$ and Fe 2p$_{1/2}$ spin orbit peaks of Fe$_3$O$_4$ [65], respectively. Compared with pristine Fe$_3$O$_4$/AC, there is no obvious change in the high-resolution scans of Fe 2p in Fe$_3$O$_4$/AC with MB loaded. Therefore, Fe$_3$O$_4$ in Fe$_3$O$_4$/AC presents weak contribution to the chemical bonding with MB, playing an important role in magnetic separation of Fe$_3$O$_4$/AC after dye removal, ensuring the easy recycle.

Fig. 7c and d show the N 1 s spectra of Fe$_3$O$_4$/AC before and after removal. The peak of C—N at 400.30 eV [66] shifts to lower binding energy position at 399.80 eV and the peak area shows a respective growth after MB adsorption. Moreover, two newly appeared peaks (—N= at 397.06 eV, =N$^+$ at 402.47 eV) are observed in Fe$_3$O$_4$/AC after MB adsorption. This result can be ascribed to the appearance of loaded MB [67]. It is notable that the peak of =N$^+$ in MB shifts from 402.00 eV to 402.47 eV, implying that the electronic transfer occurred between the =N$^+$ groups and electron obtained groups (C=O/C—O) of Fe$_3$O$_4$/AC [28,66].

For the O 1 s spectra in Fig. 7e, three peaks which are Fe—O at 530.32 eV, C—O at 531.78 eV and C=O at 533.14 eV can be observed in pristine Fe$_3$O$_4$/AC. As shown in Fig. 7f, the peak of Fe—O has no significant shift after MB removal. This result is consistent with the previous results in Fe 2p spectrum. The two shifts of C=O (from 533.14 eV to 532.62 eV) and C—O (from 531.78 eV to 531.52 eV) are observed after adsorption, suggesting the electronic transfer occurred between =N$^+$ in MB and C=O/C—O in Fe$_3$O$_4$/AC [28,66].

According to the FT-IR and XPS spectra mentioned above, the mechanism of the efficient adsorption process might be primarily due to electronic transfer between =N$^+$ in MB and C=O/C—O in Fe$_3$O$_4$/AC [28,66] as well as the π-π interaction between the skeleton sheet of Fe$_3$O$_4$/AC and aromatic ring of MB [64]. A possible adsorption mechanism figure of Fe$_3$O$_4$/AC to MB is plotted in Fig. 8.

3.4. Reuse of the adsorbent

A small neodymium magnet was used to separate the Fe$_3$O$_4$/AC from the aqueous solution within 30 seconds. Then the obtained materials were washed with ethanol and distilled water for several times. After
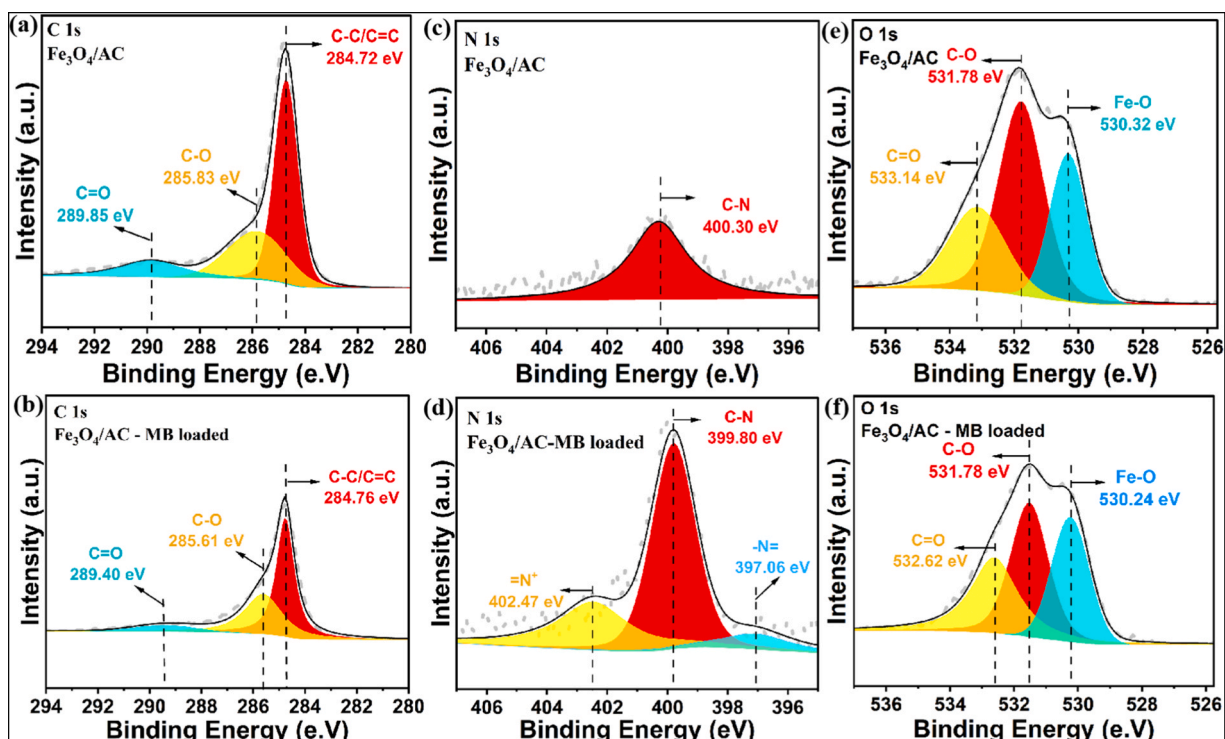
Fig. 7. The XPS spectra of C 1 s, N 1 s and O 1 s for Fe_3O_4/AC before and after adsorption.
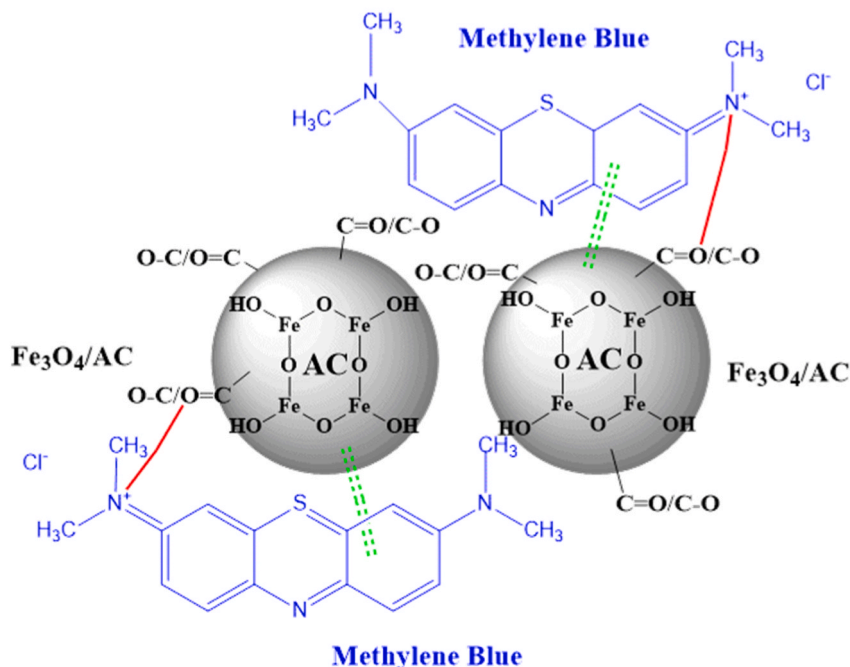
Fig. 8. Possible adsorption mechanism of MB onto Fe_3O_4/AC.

drying the materials at 60 °C for 6 h, the recycled composite was reused in another set of experiments conducted under the same conditions. Fig. 9a shows the adsorption capacities of Fe_3O_4/AC through five cycles. Notably, the adsorption capacity of Fe_3O_4/AC can also maintain at 102.4 mg/g at the fifth cycle, indicating that Fe_3O_4/AC composites in

this work have good reusability and stability for removing MB.

3.5. Application in real water samples

To imitate the removal of low concentration of MB from actual
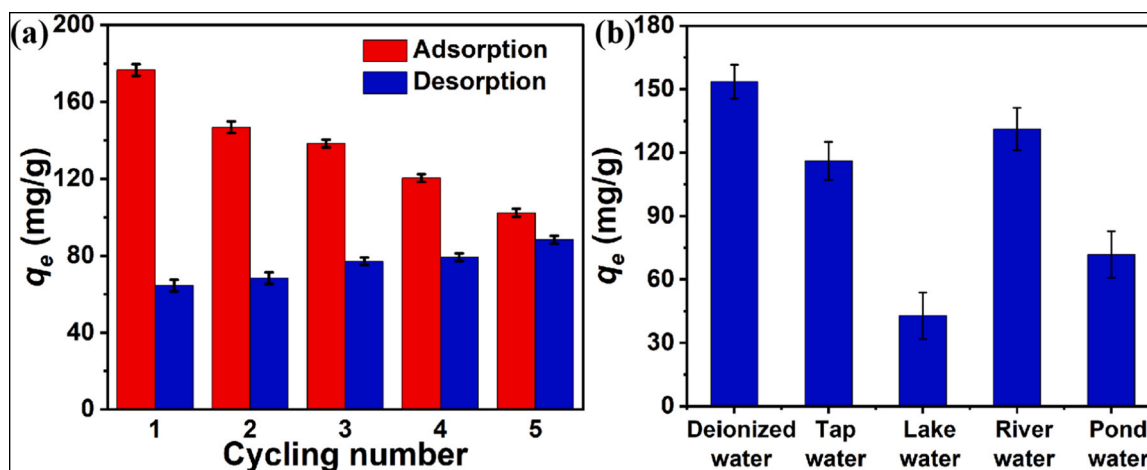
Fig. 9. (a) The reusability performance through five-cycling adsorption and desorption processes ($C_0 = 200$ mg/L, 25°C, pH = 6.5, adsorbent = 1.0 g/L, 60 min). (b) Adsorption capacity of MB from real water samples by Fe_3O_4/AC ($C_0 = 200$ mg/L, 25°C, adsorbent = 1.0 g/L, 60 min).

water, a high concentration of 200 mg/L for MB solution samples were obtained by mixing suitable MB with deionized water (pH 6.31), tap water (pH 7.64, Nanjing, China), lake water (pH 8.05, Xuanwu Lake, Nanjing, China), river water samples (pH 7.75, Qinhuai River, Nanjing, China) and the pond water (pH 8.20, Nanjing Agricultural University, Nanjing, China), respectively. The dosage of 0.1 g Fe_3O_4/AC was mixed with 100 mL of the above MB solution, which were used to investigate the actual application of Fe_3O_4/AC. As shown in Fig. 9b, the adsorption capacities of MB by Fe_3O_4/AC in actual water samples are all higher than 110 mg/g, implying that the Fe_3O_4/AC composites not only show good removal capacity in a lab settings but also have the potential to remove MB from natural environmental waters. However, it cannot be ignored that the adsorption capacities of MB by Fe_3O_4/AC in lake water and pond water were lower, which may be contributed to the various competitive impurities and organic matters in these water samples.

4. Conclusion

In this work, the Fe_3O_4/AC composites with different magnetic content were synthesized by ultrasonic mechanical blending. The mass ratio of Fe_3O_4/AC=1:5 was chosen to conduct the dye removal experiments, showing a high adsorption capacity of 251.3 ± 2.0 mg/g for MB at 20 °C and pH = 6.5 within 30 min. The adsorption process was chemical process, which was predicted by pseudo-second-order kinetics. Thermodynamic results showed the exothermic adsorption process. The purification mechanism of Fe_3O_4/AC was investigated, FT-IR results showed that MB molecules adhered to Fe_3O_4/AC after purification. According to the FT-IR and XPS results, the adsorption mechanism can be speculated to be the electronic transfer occurred between =N^+ in MB and C=O/C—O in Fe_3O_4/AC as well as the π-π interaction between the skeleton sheet of Fe_3O_4/AC and aromatic ring of MB. And the material can be recycled for 5 times, the adsorption capacity is more than 100 mg/g. The removal of MB from actual river water and tap water are effective, showing a good application prospect.

CRediT authorship contribution statement

Qin Na: Data Curation, Writing - Original Draft, Visualization. **Tian Chengxuan:** Methodology, Software. **Laura Carter:** Writing- Reviewing and Editing. **Tao Dan:** Supervision, Project administration. **Zhou Yuxin:** Validation, Investigation. **Zhang Fan:** Writing- Reviewing and Editing, Resources, Funding acquisition.

Declaration of Competing Interest

The authors declared that they have no conflicts of interest to this work. We declare that we do not have any commercial or associative interest that represents a conflict of interest in connection with the work submitted

Appendix A. Supporting information

Supplementary data associated with this article can be found in the online version at doi:10.1016/j.nxsust.2024.100057.

References

[1] S.J. Peighambardoust, D.C. Boffito, R. Foroutan, B. Ramavandi, Sono-photocatalytic activity of sea sediment@400/ZnO catalyst to remove cationic dyes from wastewater, J. Mol. Liq. 367 (2022) 120478, https://doi.org/10.1016/j.molliq.2022.120478.

[2] D. Dimbo, M. Abewaa, E. Adino, A. Mengistu, T. Takele, A. Oro, M. Rangaraju, Methylene blue adsorption from aqueous solution using activated carbon of *Spathodea campanulata*, Results Eng. 21 (2024) 101910, https://doi.org/10.1016/j.rineng.2024.101910.

[3] S. Senthilkumaar, P.R. Varadarajan, K. Porkodi, C.V. Subbhuraam, Adsorption of methylene blue onto jute fiber carbon: kinetics and equilibrium studies, J. Colloid Interface Sci. 284 (2005) 78–82, https://doi.org/10.1016/j.jcis.2004.09.027.

[4] F. Valentini, E. Cerza, F. Campana, A. Marrocchi, L. Vaccaro, Efficient synthesis and investigation of waste-derived adsorbent for water purification. Exploring the impact of surface functionalization on methylene blue dye removal, Bioresour. Technol. 390 (2023) 129847, https://doi.org/10.1016/j.biortech.2023.129847.

[5] M. Foroughi, S.J. Peighambardoust, B. Ramavandi, D.C. Boffito, Simultaneous anionic dyes degradation via H2O2 activation using Zeolite 4A/ZnO/Fe₂(MoO₄)₃ nanoparticles in a sono-photocatalytic process, Adv. Powder Technol. 35 (2024) 104320, https://doi.org/10.1016/j.apt.2023.104320.

[6] E. Onat, S. Ekinci, A new material fabricated by the combination of natural mineral perlite and graphene oxide: synthesis, characterization, and methylene blue removal, Diam. Relat. Mater. 143 (2024) 110848, https://doi.org/10.1016/j.diamond.2024.110848.

[7] A. Flilissa, K. Laouameur, N.-E. HammoudI, N. Tamam, K.K. Yadav, B. Achouri, A. Y. Alyami, O. Flilissa, J.S. Algethami, M. Abbas, B.-H. Jeon, S. Benboudiaf, Y. Benguerba, Bentonite SDBS-loaded composite for methylene blue removal from wastewater: an experimental and theoretical investigation, Environ. Res. 241 (2024) 117544, https://doi.org/10.1016/j.envres.2023.117544.

[8] M. Aaddouz, K. Azzaoui, N. Akartasse, E. Mejdoubi, B. Hammouti, M. Taleb, R. Sabbahi, S.F. Alshahateet, Removal of methylene blue from aqueous solution by adsorption onto hydroxyapatite nanoparticles, J. Mol. Struct. 1288 (2023) 135807, https://doi.org/10.1016/j.molstruc.2023.135807.

[9] T. Handayani, Emriadi Deswati, P. Ramadhani, R. Zein, Modelling studies of methylene blue dye removal using activated corn husk waste: isotherm, kinetic and thermodynamic evaluation, South Afr. J. Chem. Eng. 47 (2024) 15–27, https://doi.org/10.1016/j.sajce.2023.10.003.

[10] N.K. Amin, Removal of direct blue-106 dye from aqueous solution using new activated carbons developed from pomegranate peel: adsorption equilibrium and kinetics, J. Hazard. Mater. 165 (2009) 52–62.

[11] N.K. Amin, Removal of reactive dye from aqueous solutions by adsorption onto activated carbons prepared from sugarcane bagasse pith, Desalination 223 (2008) 152–161.

[12] N.M. Mahmoodi, R. Saleh, M. Arami, Binary system dye removal from colored textile wastewater using activated carbon: kinetic and isotherm studies, Desalination 272 (2011) 187–195.

[13] J. Rajendran, A. Panneerselvam, S. Ramasamy, P. Palanisamy, Methylene blue and methyl orange removal from wastewater by magnetic adsorbent based on activated carbon synthesised from watermelon shell, Desalin. Water Treat. 317 (2024) 100040, https://doi.org/10.1016/j.dwt.2024.100040.

[14] H. Pooladi, R. Foroutan, H. Esmaeili, Synthesis of wheat bran sawdust/Fe$_3$O$_4$ composite for the removal of methylene blue and methyl violet, Environ. Monit. Assess. 193 (2021) 276, https://doi.org/10.1007/s10661-021-09051-9.

[15] G.Z. Kyzas, E.A. Deliyanni, N.K. Lazaridis, Magnetic modification of microporous carbon for dye adsorption, J. Colloid Interfaces Sci. 430 (2014) 166–173.

[16] Z. Yang, Z. Zhao, X. Yang, Z. Ren, Xanthate modified magnetic activated carbon for efficient removal of cationic dyes and tetracycline hydrochloride from aqueous solutions, Colloid Surf. A 615 (2021) 126273.

[17] E.A. Asl, M. Haghighi, A. Talati, Enhanced simulated sunlight-driven magnetic MgAl$_2$O$_4$-AC nanophotocatalyst for efficient degradation of organic dyes, Sep. Purif. Technol. 251 (2020) 117003.

[18] W. Astuti, T. Sulistyaningsih, E. Kusumastuti, G.Y.R.S. Thomas, R.Y. Kusnadi, Thermal conversion of pineapple crown leaf waste to magnetized activated carbon for dye removal, Bioresour. Technol. 287 (2019) 121426.

[19] D. Amirhossein, Z. Mohammad, F. Morteza, A. Fatemeh, A. Hossein, Design and fabrication of core-shell magnetic and non-magnetic supported carbonaceous metal organic framework nanocomposites for adsorption of dye, J. Phys. Chem. Solids 152 (2021) 109930.

[20] B. Shabbah, Y.N. Yuliana, M.S. Noorashikin, K.N.H. Nazirah, S.A. Bakar, Review of chitosan composite as a heavy metal adsorbent: material preparation and properties, Carbohydr. Polym. 259 (2021) 117613.

[21] F.M. Valadi, A. Ekramipooya, M.R. Gholami, Selective separation of Congo Red from a mixture of anionic and cationic dyes using magnetic-MOF: experimental and DFT study, J. Mol. Liq. 318 (2020) 114051.

[22] R. Foroutan, S.J. Peighambardoust, S. Ghojavand, M. Foroughi, A. Ahmadi, F. Bahador, B. Ramavandi, Development of a magnetic orange seed/Fe$_3$O$_4$ composite for the removal of methylene blue and crystal violet from aqueous media, Biomass-.-. Conv. Bioref. (2023), https://doi.org/10.1007/s13399-023-04692-x.

[23] İ. Teğin, C. Saka, Chemical and thermal activation of clay sample for improvement adsorption capacity of methylene blue, Int. J. Environ. Anal. Chem. 103 (2023) 4503–4514, https://doi.org/10.1080/03067319.2021.1928105.

[24] S. Joshi, V.K. Garg, N. Kataria, K. Kadirvelu, Applications of Fe$_3$O$_4$@AC nanoparticles for dye removal from simulated wastewater, Chemosphere 236 (2019) 124280.

[25] M. Alizadeh, S.J. Peighambardoust, R. Foroutan, H. Azimi, B. Ramavandi, Surface magnetization of hydrolyzed Luffa Cylindrica biowaste with cobalt ferrite nanoparticles for facile Ni^{2+} removal from wastewater, Environ. Res. 212 (2022) 113242, https://doi.org/10.1016/j.envres.2022.113242.

[26] L. Fan, C. Luo, X. Li, F. Lu, H. Qiu, M. Sun, Fabrication of novel magnetic chitosan grafted with graphene oxide to enhance adsorption properties for methyl blue, J. Hazard. Mater. 215 (2012) 272–279.

[27] R. Foroutan, R. Mohammadi, J. Razeghi, M. Ahmadi, B. Ramavandi, Amendment of Sargassum oligocystum bio-char with MnFe$_2$O$_4$ and lanthanum MOF obtained from PET waste for fluoride removal: a comparative study, Environ. Res. 251 (2024) 118641, https://doi.org/10.1016/j.envres.2024.118641.

[28] R. Foroutan, R. Mohammadi, J. Razeghi, B. Ramavandi, Performance of algal activated carbon/Fe$_3$O$_4$ magnetic composite for cationic dyes removal from aqueous solutions, Algal Res. 40 (2019) 101509.

[29] J.J.S. Rabago, R.L. Ramos, J.R. Utrilla, R.O. Perez, F.J.C. Cordova, Biosorption mechanism of methylene blue from aqueous solution onto white pine (pinus durangensis) sawdust: effect of operating conditions, Sustain. Environ. Res. 27 (2017) 32–40.

[30] Ö. Şahin, M. Kaya, C. Saka, Plasma-surface modification on bentonite clay to improve the performance of adsorption of methylene blue, Appl. Clay Sci. 116–117 (2015) 46–53, https://doi.org/10.1016/j.clay.2015.08.015.

[31] F. Zhang, B. Ma, X. Jiang, Y. Ji, Dual function magnetic hydroxyapatite nanopowder for removal of malachite green and Congo red from aqueous solution, Powder Technol. 302 (2016) 207–214.

[32] G. Moussavi, R. Khosravi, The removal of cationic dyes from aqueous solutions by adsorption onto pistachio hull waste, Chem. Eng. Res. Des. 89 (2011) 2182–2189.

[33] L. Yang, Y. Zhang, X. Liu, X. Jiang, Z. Zhang, T. Zhang, L. Zhang, The investigation of synergistic and competitive interaction between dye congo red and methyl blue on magnetic MnFe$_2$O$_4$, Chem. Eng. J. 246 (2014) 88–96.

[34] R. Zhang, J. Zhang, X. Zhang, C. Dou, R. Han, Adsorption of Congo red from aqueous solutions using cationic surfactant modified wheat straw in batch mode: kinetic and equilibrium study, J. Taiwan Inst. Chem. Eng. 45 (2014) 2578–2583.

[35] F. Renault, N.M. Crini, F. Gimbert, P.M. Badot, G. Crini, Cationized starch-based material as a new ion-exchanger adsorbent for the removal of C.I. acid blue 25 from aqueous solutions, Bioresour. Technol. 99 (2008) 7573–7586.

[36] F. Zhang, X. Chen, F. Wua, Y. Ji, High adsorption capability and selectivity of ZnO nanoparticles for dye removal, Colloid Surf. A 509 (2016) 474–483.

[37] Y.S. Ho, J.C.Y. Ng, G. McKay, Kinetics of pollutant sorption by biosorbents: review, Sep. Purif. Methods 29 (2000) 189–232.

[38] M.A. Salam, R.M. El-Shishtawy, A.Y. Obaid, Synthesis of magnetic multi-walled carbon nanotubes/magnetite/ chitin magnetic nanocomposite for the removal of Rose Bengal from real and model solution, J. Ind. Eng. Chem. 20 (2014) 3559–3567.

[39] B. Huang, Y. Liu, B. Li, S. Liu, G. Zeng, Z. Zeng, X. Wang, Qi Ning, B. Zheng, C. Yang, Effect of Cu(II) ions on the enhancement of tetracycline adsorption by Fe$_3$O$_4$@SiO$_2$-Chitosan/Graphene oxide nanocomposite, Carbohydr. Polym. 157 (2016), 586–585.

[40] N. Gupta, A.K. Kushwaha, M.C. Chattopadhyaya, Adsorption studies of cationic dyes onto Ashoka (Saraca asoca) leaf powder, J. Taiwan Inst. Chem. Eng. 43 (2012) 604–613.

[41] Z.U. Ahmad, L. Yao, J. Wang, D.D. Gang, F. Islam, Q. Lian, M.E. Zappi, Neodymium embedded ordered mesoporous carbon (OMC) for enhanced adsorption of sunset yellow: Characterizations, adsorption study and adsorption mechanism, Chem. Eng. J. 359 (2019) 814–826.

[42] F. Marrakchi, M.J. Ahmed, W.A. Khanday, M. Asif, B.H. Hameed, Mesoporous-activated carbon prepared from chitosan flakes via single-step sodium hydroxide activation for the adsorption of methylene blue, Int. J. Biol. Macromol. 98 (2017) 233–239.

[43] R. Foroutan, S.J. Peighambardoust, S. Ghojavand, S. Farjadfard, B. Ramavandi, Cadmium elimination from wastewater using potato peel biochar modified by ZIF-8 and magnetic nanoparticle, Colloid Interface Sci. Commun. 55 (2023) 100723, https://doi.org/10.1016/j.colcom.2023.100723.

[44] R. Chen, J. Yu, W. Xiao, Hierarchically porous MnO$_2$ microspheres with enhanced adsorption performance, J. Mater. Chem. A 1 (2013) 11682–11690.

[45] Y.G. Pi, C.Y. Duan, Y.L. Zhou, S.J. Sun, Z.D. Yin, Z.C. Zhang, C.F. Liu, Y. Zhao, The effective removal of Congo red using a bio-nanocluster: Fe$_3$O$_4$ nanoclusters modified bacteria, J. Hazard. Mater. 127577.

[46] T.A. Saleh, Isotherm, kinetic, and thermodynamic studies on Hg(II) adsorption from aqueous solution by silica- multiwall carbon nanotubes, Environ. Sci. Pollut. Res. 22 (2015) 16721–16731, https://doi.org/10.1007/s11356-015-4866-z.

[47] L. Gan, S. Shang, E. Hu, C.W.M. Yuen, S. Jiang, Konjac glucomannan/graphene oxide hydrogel with enhanced dyes adsorption capability for methyl blue and methyl orange, Appl. Surf. Sci. 357 (2015) 866–872.

[48] S. Yang, Y. Wu, Y. Wu, L. Zhu, Optimizing decolorization of acid fuchsin and acid orange II solution by MnO$_2$ loaded MCM-41, J. Taiwan Inst. Chem. Eng. 50 (2015) 205–214.

[49] F.A. Razmi, N. Ngadi, S. Wong, I.M. Inuwa, L.A. Opotu, Kinetics, thermodynamics, isotherm and regeneration analysis of chitosan modified pandan adsorbent, J. Clean. Prod. 231 (2019) 98–109.

[50] D. Wu, P. Zheng, P. Chang, X. Ma, Preparation and characterization of magnetic rectorite/iron oxide nanocomposites and its application for the removal of the dyes, Chem. Eng. J. 174 (2011) 489–494.

[51] U.K. Sahu, S. Tripathy, N. Gouda, H.S. Mohanty, B. Dhannjaya, V.K. Choudhury, A. Sahu, A. Gouda, Eco-friendly neem leaf-based activated carbon for methylene blue removal from aqueous solution: adsorption kinetics, isotherms, thermodynamics and mechanism studies, J. Iran. Chem. SOC. 20 (2023) 2057–2067, https://doi.org/10.1007/s13738-023-02826-6.

[52] A. Mohammadi, P. Veisi, High adsorption performance of β-cyclodextrin functionalized multi-walled carbon nanotubes for the removal of organic dyes from water and industrial wastewater, J. Environ. Chem. Eng. 6 (2018) 4634–4643.

[53] F. Zhang, H. Itoh, Adsorbents made from waste ashes and post-consumer PET and their potential utilization in wastewater treatment, J. Hazard. Mater. 101 (2003) 323–337.

[54] R. Liu, X. Shen, X. Yang, Q. Wang, F. Yang, Adsorption characteristics of methyl blue onto magnetic Ni$_{0.5}$Zn$_{0.5}$Fe$_2$O$_4$ nanoparticles prepared by the rapid combustion process, J. Nanopart. Res. 15 (2013) 1679–1680.

[55] Y. Zhang, S. Shen, S. Wang, J. Huang, P. Su, Q. Wang, B. Zhao, A dual function magnetic nanomaterial modified with lysine for removal of organic dyes from water solution, Chem. Eng. J. 239 (2014) 250–256.

[56] M. Alizadeh, S.J. Peighambardoust, R. Foroutan, Efficacious adsorption of divalent nickel ions over sodium alginate-g-poly(acrylamide)/hydrolyzed Luffa cylindrica-CoFe$_2$O$_4$ bionanocomposite hydrogel, Int. J. Biol. Macromol. 254 (2024) 127750, https://doi.org/10.1016/j.ijbiomac.2023.127750.

[57] A. Wei, B. Liu, H. Zhao, Y. Chen, W. Wang, Y. Ma, H. Yang, S. Liu, Synthesis and formation mechanism of flowerlike architectures assembled from ultrathin NiO nanoflakes and their adsorption to malachite green and acid red in water, Chem. Eng. J. 239 (2014) 141–148.

[58] Z. Wu, R. Li, L. Pei, Y. Yang, X. Li, J. Jiang, F. Zhang, Easily modified barium phosphate composites for effective removal of methyl blue from solution, J. Environ. Chem. Eng. 9 (2021) 105423.

[59] R. Das, V.S. Sypu, H.K. Paumo, M. Bhaumik, V. Maharaj, A. Maity, Silver decorated magnetic nanocomposite (Fe$_3$O$_4$@PPy-MAA/Ag) as highly active catalyst towards reduction of 4-nitrophenol and toxic organic dyes, Appl. Catal. B Environ. 244 (2019) 546–558.

[60] D. Nagaonkar, S. Gaikwad, M. Rai, Catharanthus roseus leaf extractsynthesized chitosan nanoparticles for controlled in vitro release of chloramphenicol and ketoconazole, Colloid Polym. Sci. 293 (2015) 1465–1473.

[61] Z. Song, F. Lian, Z. Yu, L. Zhu, B. Xing, W. Qiu, Synthesis and characterization of a novel MnOx-loaded biochar and its adsorption properties for Cu2+ in aqueous solution, Chem. Eng. J. 242 (2014) 36–42.

[62] R.A. Reza, M. Ahmaruzzaman, A novel synthesis of Fe$_2$O$_3$@activated carbon composite and its exploitation for the elimination of carcinogenic textile dye from an aqueous phase, RSC Adv. 5 (2015) 1575–1586.

[63] Y. Zhang, P. He, Y. Zhang, H. Chen, A novel electroconductive graphene/fly ash-based geopolymer composite and its photocatalytic performance, Chem. Eng. J. 334 (2018) 2459–2466.

[64] G.Z. Kyzas, E.A. Deliyanni, N.K. Lazaridis, Magnetic modification of microporous carbon for dye adsorption, J. Colloid Interfaces Sci. 430 (2014) 166–173.

[65] T. Yamashita, P. Hayes, Analysis of XPS spectra of Fe^{2+} and Fe^{3+} ions in oxide materials, Appl. Surf. Sci. 254 (2008) 2441–2449.

[66] Z. Zhang, X. Xu, Wrapping carbon nanotubes with poly (sodium 4-styrenesulfonate) for enhanced adsorption of methylene blue and its mechanism, Chem. Eng. J. 256 (2014) 85–92.

[67] A.V. Naumkin, A. Kraut-Vass, S.W. Gaarenstroom, C.J. Powell, NIST X-ray photoelectron spectroscopy database, ⟨http://srdata.nist.gov/xps/Default.aspx⟩ (2012).